WATER ON MARS: INSIGHTS FROM NOMINALLY ANHYDROUS PYROXENE IN LAFAYETTE, NAKHLA, AND NORTHWEST AFRICA 7034. J. Davidson[1,2,*], M. Wadhwa[2], and R. L. Hervig[2], [1]Center for Meteorite Studies, Arizona State University, 781 East Terrace Road, Tempe, AZ 85287-6004, USA. [2]School of Earth and Space Exploration, Arizona State University, 781 East Terrace Road, Tempe, AZ 85287-6004, USA. *Email: jdavidson@asu.edu

Introduction: Determining the source(s) of planetary water via the analysis of the hydrogen isotope compositions of martian meteorites is complicated by overprinting of geologic and atmospheric processes on Mars, shock metamorphism during ejection from Mars, and terrestrial weathering on Earth [1]. As Mars has no plate tectonics, crustal material, which likely exchanged at least some water with the martian atmosphere, is not recycled into the mantle keeping the water reservoirs in the mantle and atmosphere mostly isolated, buffered by a potential third reservoir in the crust [2]. The clinopyroxenites Lafayette and Nakhla provide opportunities to investigate the H systematics of martian samples whose igneous minerals may contain magmatic water (e.g., [3]). In contrast, the regolith breccia Northwest Africa (NWA) 7034 and its paired samples, the only known samples with compositions representative of the average martian crust [4], allow us to investigate the water content and hydrogen isotopic composition of the martian crust. Furthermore, Nakhla and NWA 7034 are among the least-shocked martian samples available for study (<20 GPa [5] and 5 to 15 GPa [6], respectively).

Many previous studies of volatiles in martian meteorites have focused on determining the H isotope ratios (expressed as δD) and H_2O contents of the hydrated mineral apatite [e.g., 3,7]. Late-formed apatite crystallizes from highly fractionated melt that may have undergone other processes such as degassing while earlier-formed primary igneous minerals, such as pyroxene, may be more reliable for determining the δD–H_2O systematics of their parent magmas. As such, we target nominally anhydrous pyroxene in this study. Pyroxene is abundant in the clinopyroxenites Lafayette and Nakhla [8] and occurs in the groundmass and a variety of clastic igneous lithologies in NWA 7034 including Fe-, Ti-, and P-rich (FTP) clasts and basaltic clasts [4,9]. These samples provide the opportunity to compare the H isotope compositions and H_2O contents of different lithologies within the crustal breccia and between different geologic settings on Mars.

Analytical Methods: Interior, fusion-crust free samples of Lafayette (one chip), Nakhla (one chip), and NWA 7034 (two chips) were each co-mounted with terrestrial standards in indium metal in four aluminum discs; no water was used during sample preparation. Quantitative compositional analyses of pyroxene were obtained with a Cameca SX-100 electron probe microanalyzer (EPMA) at the University of Arizona's Lunar and Planetary Laboratory (operating conditions: 20 kV and 20 nA) while high-resolution secondary and backscattered electron (BSE) imaging was undertaken on a JEOL JXA-8530F EPMA at Arizona State University (ASU) before and after isotopic analysis (operating conditions: 20 kV and 15 nA). Secondary ion mass spectrometry (SIMS) measurements of H isotope compositions and H_2O contents of pyroxenes were performed on the Cameca IMS-6f at ASU using analytical protocols similar to those described in [7]. A Cs^+ primary beam (~15 nA) was rastered over a ~40 × 40 μm^2 area (a field aperture limited the analyzed area to the central 15 μm to reduce background H counts associated with crater edges). Each measurement run consisted of 50 to 100 consecutive cycles (depending on H abundance), each consisting of measuring H^- and D^- with counting times of 1 s and 10 s, respectively. The $^{16}O^-$ peak was measured at the end of each run to determine the $H^-/^{16}O^-$ ratio used for determination of H_2O content. The H_2O concentrations were estimated using a $H^-/^{16}O^-$ vs. H_2O calibration curve on terrestrial standards. Background H_2O concentrations during each analytical session (7 ppm for Lafayette; 10 and 18 ppm for Nakhla; 9 and 19 ppm for NWA 7034), determined by analyses of nominally anhydrous San Carlos olivine and dry PMR53 pyroxene, were corrected for via the method of [10]. Instrumental mass fractionation was monitored throughout analytical sessions using terrestrial pyroxene and basaltic glass standards.

Results: *Lafayette.* Pyroxenes in Lafayette occur as minimally fractured, large crystals (up to ~800 μm diameter; Fig. 1a) with heavy H isotope compositions (δD = 840 ± 60 ‰ to 1630 ± 120 ‰) and low H_2O contents (~10 ± 2 ppm to 30 ± 6 ppm) (Fig. 2a).

Nakhla. Pyroxenes in Nakhla are similar in appearance to those in Lafayette (up to ~900 μm diameter; Fig. 1b), have heavy H isotope compositions (δD = 310 ± 170 ‰ to 1440 ± 120 ‰), and low H_2O contents (<10 ± 2 ppm to 90 ± 17 ppm) (Fig. 2a).

Northwest Africa 7034. Most pyroxenes in NWA 7034 occur as large orthopyroxene phenocrysts in the groundmass (up to 700 μm diameter; Fig. 1c,d), have light H isotope compositions (δD = –160 ± 12 ‰ to 275 ± 220 ‰), and high H_2O contents (40 ± 8 ppm to

~2240 ± 500 ppm) compared to nakhlite pyroxenes (Fig. 2). Pyroxenes were also analyzed in a basaltic clast (<60 µm diameter; δD = 260 ± 70 ‰ to 290 ± 60 ‰; ~330 ± 65 ppm to 910 ± 180 ppm H_2O; Fig. 1e) and an FTP clast (~300 µm diameter; δD = 130 ±110 ‰ to 330 ± 110 ‰; ~100 ± 20 ppm to 900 ± 180 ppm; Fig. 1f).

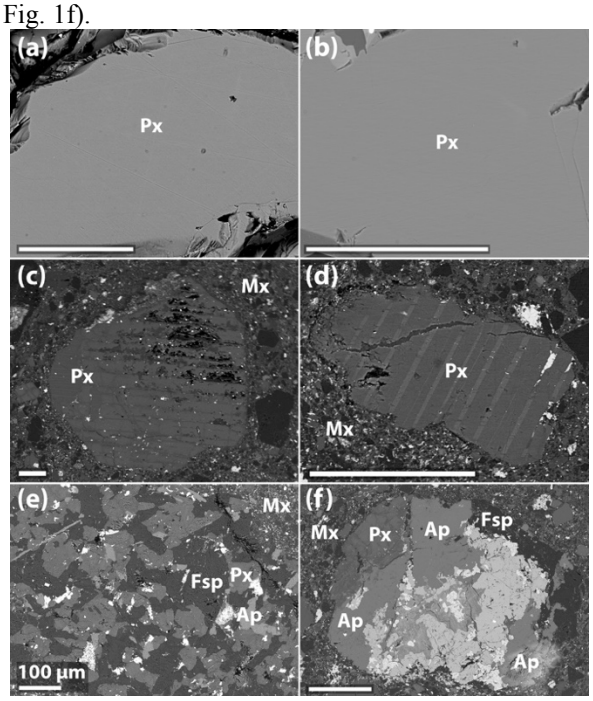

Fig. 1: *BSE images of pyroxene (Px) in (a) Lafayette, (b) Nakhla, and (c,d) interclastic matrix (Mx), (e) a basaltic clast, and (f) an FTP clast in NWA 7034. Ap = apatite, Fsp = feldspar. All scale bars are 100 µm.*

Discussion: The H_2O contents of some NWA 7034 pyroxenes are higher than those reported for clinopyroxene in the shergottite Tissint (1300 ± 200 ppm H_2O [14]) (Fig. 2b) and are generally much higher than seen in the nakhlite pyroxenes. Since the nakhlites and NWA 7034 were prepared via the same anhydrous method, it seems unlikely that this water was introduced during sample preparation. It is also unlikely that the highest H_2O contents in NWA 7034 pyroxenes were incorporated during crystallization. They may, however, be explained by post-eruption addition of water on Mars, which was proposed to explain the H_2O-rich grain rims observed in apatite from NWA 7034 [12].

Pyroxenes in Lafayette, Nakhla and NWA 7034 exhibit an inverse relationship between H isotope compositions and H_2O contents. This is consistent with the trend seen previously in NWA 7034 apatites [7,12] and Nakhla pyroxenes [13]. Such a trend may result from degassing via dehydrogenation (i.e., H_2 loss), which typically leads to isotopically heavier δD and an inverse relationship between δD and H_2O concentrations (e.g., [11]). Alternatively, it may be from mixing between two distinct reservoirs (i.e., one with high δD and low H_2O content, and the other with low δD and high H_2O content).

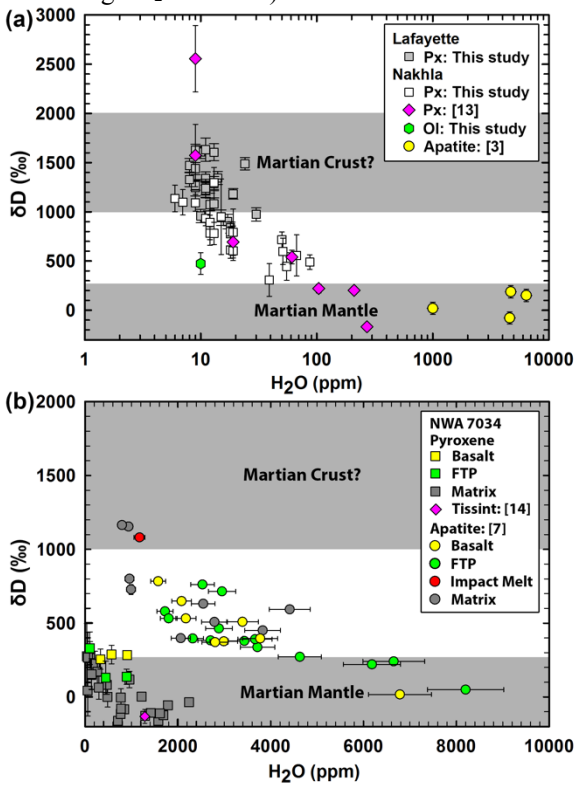

Fig. 2: *H-isotope compositions (δD in per mil) versus water concentrations (H_2O in ppm) of anhydrously-prepared pyroxenes from (a) Lafayette and Nakhla (compared with published Nakhla data [3,13]), and (b) various lithological settings in NWA 7034 (compared with Tissint pyroxene [14] and our previous apatite data [7]). Fields representing the mantle (<275 ‰ [3,15,16]) and proposed crustal reservoir (δD = 1000–2000‰ [2]) are also shown.*

Acknowledgments: This work was supported by the NASA SSW grant NNX16AT37G to M.W.

References: [1] Hallis L. J. et al. (2017) *Phil. Trans. R. Soc. A.*, *375*, 20150390. [2] Usui T. et al. (2015) *EPSL, 410*, 140–151. [3] Hallis L. J. et al. (2012) *EPSL, 359–360*, 84–92. [4] Agee C. B. et al. (2013) *Science, 339*, 780–785. [5] Greshake A. (1998) *MAPS, 33*, A63. [6] Wittman A. et al. (2015) *MAPS, 50*, 326–352. [7] Davidson J. et al. (2019) *LPS L,* #1596. [8] Treiman A. H. (2005) *CEG, 65,* 203–270. [9] Santos A. R. et al. (2015) *GCA, 157*, 56–85. [10] Mosenfelder J. L. et al. (2011) *AM*, *96*, 1725–1741. [11] Demény A. et al. (2006) *RCMS, 20,* 919–925. [12] Hu S. et al. (2019) *MAPS*, *54*, 850–879. [13] Peslier A. H. et al. (2019) *GCA*, *266*, 382–415. [14] Hallis L. J. et al. (2017) *GCA, 200*, 280–294. [15] Usui T. et al. (2012) *EPSL, 357–358*, 119–129. [16] Mane P. et al. (2016) *MAPS*, *51*, 2073–2091.